ELSEVIER

Numerical study of liquid film cooling in a rocket combustion chamber

H.W. Zhang, W.Q. Tao *, Y.L. He, W. Zhang

State Key Laboratory of Multiphase Flow in Power Engineering, Xi'an Jiaotong University, Xi'an, China

Abstract

A numerical study is reported to investigate the liquid film cooling in a rocket combustion chamber. Mass, momentum and heat transfer characteristics through the interface are considered in detail. A marching procedure is employed for solution of the respective governing equations for the liquid film and gas stream together. The standard turbulence k–ε model is used to simulate the turbulence gas flow and a modified van Driest model is adopted to simulate the turbulent liquid film flow. Radiation of gas stream is also considered and simulated with the flux model. Downstream of the liquid film the gaseous film cooling is numerically studied simultaneously. Results are presented for a mixed gases–water system under different condition. Various effects on the liquid film length are examined in detail. There is a good agreement between the numerical prediction and experimental result on the liquid film length.
© 2005 Elsevier Ltd. All rights reserved.

1. Introduction

Liquid film cooling provides an attractive means of protecting the surface of combustion chamber wall from thermal damage of a hot gas stream. A thin continuous liquid layer is injected between the wall surface and the hot gas stream and forms an annular flow as showed in Fig. 1. Heat transfers from the hot gases stream to the liquid film by both radiation and convection. This energy is absorbed in heating and vaporizing the liquid in the protective film on the wall.

The studies of liquid film cooling have been carried out by a number of investigators. Examples include the investigation of the physical characteristics of the gas–liquid interface such as interfacial structure and film

instability [1,2]. Some experiment and analysis results have been reported in [3–6]. In these predictions the details of transport process in the boundary layer have not been taken into account.

The application of the liquid film cooling is generally related to high rates of heat transfer and evaporation of liquid film at the interface. The laminar and turbulent forced convection boundary layer type air–vapor flows over a vaporizing liquid film on a flat plate or in a tube have been numerically studied [7–10]. In these analyses, the liquid film on the wetted wall was assumed to be extremely thin so that its thickness is neglected and it is only regarded as a boundary condition for the heat and mass transfer.

The effects of the momentum and energy transports in the liquid film on the heat and mass transfer in the gas flow have been considered in the studies of Shembharkar and Pai [11], Baumann and Thiele [12] and He et al. [13]. In these investigations some assumptions

---

* Corresponding author.
E-mail address: wqtao@mail.xjtu.edu.cn (W.Q. Tao).

Nomenclature

c	mass fraction of vapor
c_p	specific heat, J kg K^{-1}
D	mass diffusivity, m^2 s^{-1}
k	turbulent kinetic energy, m^2 s^{-2}
$\dot{m}_I$	interfacial mass flux, kg m^{-2} s^{-1}
M_a	molar mass of air, kg mol^{-1} K^{-1}
M_v	molar mass of vapor, kg mol^{-1} K^{-1}
p	mixture pressure, Pa
Pr	Prandtl number
r	coordinate in r-direction, m
S_r	source of radiation, W m^{-3}
T	temperature, K
u	axial velocity, m s^{-1}
v	radial velocity, m s^{-1}
x	axial coordinate, m

Greek symbols

ε	the rate of the dissipation of turbulent energy, m^2 s^{-3}

Γ_0	inlet liquid mass flow, kg m^{-1} s^{-1}
δ	local liquid film thickness, m
γ	latent heat of vaporization, J kg^{-1}
λ	thermal conductivity, W m^{-1} K^{-1}
η	dynamic viscosity, kg m^{-1} s^{-1}
v	kinematics viscosity, m^2 s^{-1}
ρ	density, kg m^{-3}

Subscripts

0	condition at inlet
a	gas
G	mixture (gas + vapor)
I	condition at gas–liquid interface
L	liquid film
out	outer coolant
r	radiation
t	turbulent
v	of vapor
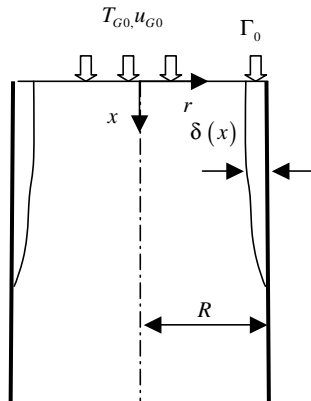
Fig. 1. Schematic diagram of the physical system.

made by Nusselt [14] for the analysis of film condensation were adopted to simplify the treatment about the transports in the liquid film. The more detailed analyses of the transport processes in the liquid film were performed by some investigators [15–19]. In all these studies, the flow in the liquid film was assumed to be very low such that the inertia term of the liquid film was neglected.

In the process of liquid film cooling, the Reynolds number ($Re_l = 4\Gamma_0/\eta$) of the liquid film flow in the entrance is generally much greater than the critical value of 1500 for laminar condition quoted by Ueda and Tanaka [1]. However, in all the above investigations the flow was assumed to be laminar. The effects of turbu-

lence of the liquid film on the momentum and energy transfers in the liquid film were analyzed by Yih and Liu [20]. Similar studies were carried out by Yan [21], Yan and Soong [22,23], Yan [24], Fedorov et al. [9] and He et al. [13]. In the study of Yan [21], the flow in the gas stream was assumed to be laminar, while in the study of Yan and Soong [22,23] the inertia term in the momentum equation of liquid film was neglected. In the turbulent studies mentioned above, the gas stream Reynolds number is not very high, usually in the order of 10^4–10^5, hence the laminar sublayer is not thin. Thus the low-Reynolds number k–ε turbulence model which requires enough grid points to be arranged in the sublayer was applied to simulate the turbulent gas flow. For the case of gas flow in a rocket combustion chamber, the Reynolds-number of the gas flow is very high, often up to 10^7 or higher. In such situation, the low-Reynolds number turbulent model is too expensive to be used because the very thin laminar sublayer will require tremendous grid points in radial direction. Instead, a standard k–ε modal with wall-function strategies will be practical and applicable.

The studies of [21–24] all focused on the heat and mass transfer at the interface. Neither the effects of the radiation nor the external cooling was considered. Moreover, the gas temperature and pressure were too low to reveal truly the huge heat flux characteristics of the gases in a practical combustion chamber. In practical situations, temperature of the gases in the combustion chamber is so high that the radiation and gas dissociation should not be neglected. Furthermore, the

transpiration of vapor from the liquid film decreases the normally expected convective flux that makes the radiation being more significant. Therefore the influence of radiation on the film cooling should be taken into account together with the convective heat transfer. The external cooling, whose effects on the rocket combustion chamber heat transfer are important, is also considered in the present paper. The liquid film cooling length is an important parameter for liquid film cooling design in a rocket combustion chamber and is another major concern of this paper, on which not enough attention had been paid in Refs. [21–24]. Thus the results obtained in [21–24] are not good enough to describe the actual performance of liquid film in a practical combustion chamber.

In the present study, attention is mainly concentrated on the phenomena that characterize the exchange of heat and mass transfer between a hot gas stream and a thin liquid film. The effects of gaseous radiation, external cooling and high temperature and high pressure of gases are all taken into account to reveal the characteristics of liquid film cooling in a rocket combustion chamber. In the following, the physical and numerical model will first be presented, followed by the turbulence model and radiation model. Then the determination of the gas thermophysical properties and numerical approach will be described. In the presentation of the numerical results, a comparison between present numerical prediction and the data available in the literature will first be provided, followed by the discussion of local heat flux, local wall temperature distribution, the effects of Reynolds number and the external cooling condition on the length of liquid film. Finally some conclusions will be drawn.

2. Mathematical formulation

2.1. Physical model and assumptions

Consider a liquid film cooling in a combustion chamber shown schematically in Fig. 1. The thin liquid film is fed with inlet liquid temperature T_{L0} and inlet coolant flow rate Γ_0. The walls are either thermally insulated or cooled by regeneration cooling. The mixture gases flow enters the chamber with a fully developed velocity profile $u_0(r)$, uniform temperature T_0 and concentration c_0. The transport processes are considered steady and the flow is incompressible. In order to concentrate our attention on the most important factors and neglect some secondary effects the following additional assumptions are made in our analysis.

(1) Combustion process is completed instantaneously and sufficiently, and the free stream gas consists of the combustion products of fuel/oxygen.

(2) Viscous dissipation effect is negligible.
(3) The gas–liquid interface is at the state of thermodynamic equilibrium.
(4) The axial diffusion and radiation are neglected in comparison with the radial diffusion and radiation.
(5) The gas–liquid interface is smooth and waveless.

2.2. Governing equations

The time-averaged Navier–Stokes equations for the incompressible steady two-dimensional parabolic type flow in the cylindrical coordinates can be written as follows:

Continuity equation of the liquid film

$$(1/r)\partial(r\rho_L v_L)/\partial r + \partial(\rho_L u_L)/\partial x = 0 \tag{1}$$

Axial momentum equation of the liquid film

$$(1/r)\partial(r\rho_L v_L u_L)/\partial r + \partial(\rho_L u_L u_L)/\partial x \\ = -\mathrm{d}p/\mathrm{d}x + (1/r)\partial(r(\eta_L + \eta_{Lt})\partial u_L/\partial r)/\partial r \tag{2}$$

Energy equation of the liquid film

$$(1/r)\partial(r\rho_L c_{pL} v_L T_L)/\partial r + \partial(\rho_L c_{pL} u_L T_L)/\partial x \\ = (1/r)\partial(r(\lambda + \lambda_{Lt})\partial T_L/\partial r)/\partial r \tag{3}$$

Continuity equation of the gas flow

$$(1/r)\partial(r\rho_G v_G)/\partial r + \partial(\rho_G u_G)/\partial x = 0 \tag{4}$$

Axial momentum equation of the gas flow

$$(1/r)\partial(r\rho_G v_G u_G)/\partial r + \partial(\rho_G u_G u_G)/\partial x \\ = -\mathrm{d}p/\mathrm{d}x + (1/r)\partial(r(\eta_G + \eta_{Gt})\partial u_G/\partial r)/\partial r \tag{5}$$

Energy equation of the gas flow

$$(1/r)\partial(r\rho_G c_{pG} v_G T_G)/\partial r + \partial(\rho_G c_{pG} u_G T_G)/\partial x \\ = (1/r)\partial(r(\lambda_G + \lambda_{Gt})\partial T_G/\partial r)/\partial r \\ + \rho_G D(c_{pv} - c_{pa})/c_{pG}\partial T_G/\partial r\partial c/\partial r + S_r \tag{6}$$

Concentration equation of vapor

$$(1/r)\partial(r\rho_G v_G c)/\partial r + \partial(\rho_G u_G c)/\partial x \\ = (1/r)\partial(r\rho_G(D + D_t)\partial c/\partial r)/\partial r \tag{7}$$

At every axial location, the overall mass balance between the gas flow and liquid film should be satisfied:

$$\rho_G u_0(R - \delta_0)^2/2 = \int_0^{R-\delta} r\rho_G u_G \,\mathrm{d}r + \int_0^x \rho_G v_I \,\mathrm{d}x \tag{8}$$

$$\Gamma_0 = \int_{R-\delta}^R (r\rho u \,\mathrm{d}r)_L - \int_0^x \rho_G v_I \,\mathrm{d}x \tag{9}$$

2.3. Boundary conditions

$$x = 0 : \quad u_G = u_{G0}, \quad T_G = T_{G0}, \quad c = c_0,$$
$$u_L = u_{L0}, \quad T_L = T_{L0} \tag{10}$$
$$r = 0 : \quad \partial u_G/\partial r = 0, \quad \partial c/\partial r = 0,$$
$$v_G = 0, \quad \partial T_G/\partial r = 0 \tag{11}$$
$$r = R : \quad u_L = 0, \quad v_L = 0,$$
$$(\lambda_L + \lambda_{Lt})\partial T_L/\partial r = h(T_w - T_{out}) \tag{12}$$

2.4. Interfacial matching conditions

(a) Continuities of velocity and temperature

$$u_I(x) = u_{G,I} = u_{L,I}, \quad T_I(x) = T_{G,I} = T_{L,I} \tag{13}$$

(b) Continuity of shear stress

$$\tau_I = [(\eta + \eta_t)\partial u/\partial r]_{G,I} = [(\eta + \eta_t)\partial u/\partial r]_{L,I} \tag{14}$$

(c) Interface radial velocity

The radial velocity component is non-zero due to the generation of vapor at the interface. Since the gas–liquid interface is semi-permeable, that is, the solubility of gas into the water is negligible, the gas does not move to the interface in radial direction, and the velocity of the gases–vapor mixture can be calculated by:

$$v_I = -(D + D_t)/(1 - c_I)\partial c/\partial r \tag{15}$$

(d) Interface vapor mass fraction

According to assumption (3), the mass fraction of the vapor can be evaluated by:

$$c_I = M_v P_{v,I}/[M_a(P - P_{v,I}) + M_v P_{v,I}] \tag{16}$$

(e) Mass flux of vaporized liquid into the gas flow

$$\dot{m}_I = \rho_G(D + D_t)/(1 - c_I)\partial c/\partial r \tag{17}$$

(f) Energy balance at the gas–liquid interface

$$[(\lambda + \lambda_t)\partial T/\partial r]_{L,I} + q_{r,I} = [(\lambda + \lambda_t)\partial T/\partial r]_{G,I} + \dot{m}_I \gamma \tag{18}$$

2.5. Turbulence model

2.5.1. Liquid film turbulence model

To simulate momentum and heat transfer of the liquid film, a modified Van Driest model proposed by Yih and Liu [20] is used herein. Similar models have been applied to analyze momentum and heat transfer across a turbulent liquid film in some previous studies [21–23]. The details of the model are presented below:

For $y/\delta \leqslant 0.6$

$$\eta_{Lt}/\eta_L = -0.5 + 0.5\{1 + 0.64(y^+)^2(\tau/\tau_w)$$
$$\times [1 - \exp(-y^+(\tau/\tau_w)^{1/2}/A^+)]^2 f^2\}^{1/2} \tag{19}$$

For $0.6 < y/\delta \leqslant 1.0$

$$\eta_{lt} = \eta_{lt}|_{y/\delta=0.6} = \text{constant} \tag{20}$$

The turbulent conductivity is written as:

$$\lambda_{Lt} = \eta_{Lt} c_{pL}/Pr_t \tag{21}$$

2.5.2. Gas flow turbulence model

For simulation of turbulent flow of the gas, the standard k–ε model is adopted. The transport equations of k and ε are as follows:

$$(1/r)\partial(r\rho v k)/\partial r + \partial(\rho u k)/\partial x$$
$$= (1/r)\partial[r(\eta + \eta_t/\sigma_k)\partial k/\partial r]/\partial r + \eta_t(\partial u/\partial r)^2 - \rho\varepsilon \tag{22}$$

$$(1/r)\partial(r\rho v \varepsilon)/\partial r + \partial(\rho u \varepsilon)/\partial x$$
$$= (1/r)\partial[r(\eta + \eta_t/\sigma_\varepsilon)\partial\varepsilon/\partial r]/\partial r$$
$$+ C_1(\varepsilon/k)\eta_t(\partial u/\partial r)^2 - C_2\rho\varepsilon^2/k \tag{23}$$

where $\eta_t = \rho C_\mu k^2/\varepsilon$ and $C_\mu = 0.09$, $C_1 = 1.4$, $C_2 = 1.8$, $\sigma_k = 1.0$, $\sigma_\varepsilon = 1.3$, $\sigma_t = 0.9$.

2.6. Radiation model

To calculate the radiation of gases, the FLUX model is adopted [25]. The chamber is assumed to be an infinite cylinder, so the radiation of axial direction can be neglected. Then the radiation heat flux of radial direction can be expressed as

$$dq_r^+/dr = -(a + \sigma_s)q_r^+ + aE_b + (\sigma_s/2)(q_r^+ + q_r^-)$$
$$- (q_r^+ - q_r^-)/r \tag{24}$$
$$dq_r^-/dr = (a + \sigma_s)q_r^- - aE_b - (\sigma_s/2)(q_r^+ + q_r^-) \tag{25}$$

where q_r^+ and q_r^- are the radiation heat flux pointing to the wall and the center respectively.

The boundary condition for the radiation heat flux is as follows:

$$r = 0 : \quad q_r^+ = q_r^- \tag{26}$$
$$r = R : \quad q_{r,w}^- = \varepsilon_w E_{bw} + (1 - \varepsilon_w)q_{r,w}^+ \tag{27}$$

The gas radiation heat flux is treated as an additional source term [26] of the energy governing equation and it can be expressed by

$$S_r \equiv \Phi_r = -(1/r)d(rq_r^+ - rq_r^-)/dr \tag{28}$$

2.7. Thermophysical properties

To compare the present results with the experimental results of Morrell [27], the film cooling with stream of ternary gases mixture (water vapor–nitrogen–oxygen) is investigated. The thermophysical properties of the mixture gases (water vapor, nitrogen and oxygen)

Table 1
Comparisons of L_{film} for various grid arrangements for a typical case

Wall function 1			Wall function 2		
$I \times J \times K$	y^+	L_{film} (m)	$I \times J \times K$	y^+	L_{film} (m)
$200 \times 112 \times 40$	16	0.199	$200 \times 92 \times 40$	42	0.187
$100 \times 102 \times 20$	23	0.195	$100 \times 92 \times 20$	42	0.189
$100 \times 92 \times 20$	36.5	0.188	$100 \times 82 \times 20$	57	0.191
$100 \times 82 \times 20$	57.5	0.177	$100 \times 72 \times 20$	78	0.191
$50 \times 82 \times 20$	57.5	0.177	$50 \times 72 \times 20$	78	0.190

I: total grid points in the axial direction; J: total grid points in the transverse direction at the gas side; K: total grid points in the transverse direction at the liquid side; y^+: averaged value of all the near-wall nodal points dimensionless distance.

depend on temperature and concentrations. They are calculated from the pure component data by means of mixing rules applicable to any multicomponent mixture. The pure component and phase equilibrium data are taken from Vargaftik [28] and are approximated by polynomials in term of temperature for a fixed pressure. The dynamic viscosity η is computed according to the formula of Wilke [29], the thermal conductivity λ is expressed with the relation of Lindsay and Bromley [29], and the diffusion coefficient D of water vapor in the mixture is taken from Hirschfelder [29]. For further details of the thermophysical properties the work of Reid and Sherwood [29] can be referred.

3. Solution method

The parabolic type governing equations (1)–(7) are solved by the finite volume method. The matching condition imposed at the gas–liquid interface, Eq. (18), is dealt with by using additional source term method [26]. The axial convection terms are discretized by the fully implicit scheme and the radial convection and diffusion terms are approximated by the central difference. Each of the discretized equations forms a tridiagonal matrix equation, which can be solved by the TDMA. Radiation equations (24) and (25) are solved by the fourth-order Runge–Kutta method.

The numerical solution is advanced forward step by step, and the computational procedure may be summarized as follows:

1. For any axial location x, assume values of dp/dx and δ_x.
2. Solve the discretized forms of Eqs. (2) and (5) simultaneously for u.
3. Numerically integrate Eqs. (1) and (4) to find v.
4. Solve the discretized forms of Eqs. (3), (6), (7), (22) and (23) simultaneously for t, c, k, ε.
5. Check the mass conservation of both liquid film and gas flow by examining the satisfaction of Eqs. (8) and (9). If not, adjust dp/dx and δ_x and repeat Steps 2–5.

6. Check the satisfaction of the convergence of velocity, temperature, mass fraction, turbulent kinetic energy and dissipation. If the relative error between two consecutive iterations is less than the specified value, stop, i.e., if:

$$\max(|\phi_{i,j}^n - \phi_{i,j}^{n-1}|/|\phi_{i,j}^n|) < \varepsilon_\phi \qquad (29)$$

the iteration is regarded convergence, where ϕ represents the variables u, t, c, k, ε. If not, repeat Steps 1–6.

To enhance computational accuracy with given number of grids, the grids are distributed non-uniformly in axial and in radial directions in the gases flow region. The grids are compressed towards the gas–liquid interface and towards the entrance of the chamber.

To obtain grid-independent results, numerical experiments for two different wall functions and several grid arrangements are performed and a comparison of the liquid film length for a typical case is shown in Table 1. It is found from Table 1 that the numerical results of wall function 1 [30] are more sensitive to the value of y^+ than wall function 2 [31]. The deviations of the results of wall function 2 at the two grids systems of $200 \times 92 \times 40$ and $50 \times 72 \times 20$ were always less than 2%. Therefore, the wall function 2 and the $50 \times 72 \times 20$ grid system are chosen for the subsequent computations.

4. Results and discussion

4.1. Comparison of the present prediction with experiment

In view of the unavailability of recent experimental data, some experimental data for liquid film cooling in the rocket combustion chamber reported in early years [5] is cited and compared in the present study. In the Morrell's report [27] detailed experimental data had been provided, including the liquid film length. Morrell's tests were performed in a 4-inch diameter chamber with liquid–oxygen and ammonia propellants. The liquid coolant was injected 2.8 inches downstream of the propellant injector. Water, ethanol and ammonia were

Table 2
Comparisons of L_{film} of measurements and computations for several cases

Case	O/F	T_g (K)	P (atm)	G (kg/s m^2)	Γ (kg/s m)	L_{meas} (m)	L_{comp} (m)
1	1.61	2950	17.4	226	0.269	0.212	0.190
2	1.5	2963	17.0	207	0.209	0.162	0.146
3	1.72	2935	17.5	220	0.128	0.0986	0.0808
4	1.67	2942	17.7	224	0.296	0.217	0.216

O/F: the mass ratio of oxygen to fuel; T_g: the free steam gas temperature; P: pressure of combustion chamber; G: gas mass flow rate per area; Γ: liquid coolant mass flow rate per length; L_{meas}: the measured liquid film length; L_{comp}: the computational liquid film length.

tested as coolants. The ammonia was at super-critical condition and the liquid coolant flow in all of the ethanol tests greatly exceeded Knuth's critical value for the formation of large waves in liquid film, hence only the data about water coolant were adopted here.

A comparison of our computational results with the experimental data for four typical tests is given in Table 2. From Table 2 it can be found that the relative deviations of the computational liquid film length ranged from 0.5% to 18%, and the longer the liquid film length, the less the relative deviation. The more significant deviation for short liquid film length is attributed to the effects of the inlet on heat transfer. The longer the liquid film length, the less influence the inlet condition. Our assumptions of uniform gas inlet temperature and developed velocity distribution may be different from the test conditions of Morrell [27]. Since no details were given for the inlet condition in Morrell's test data, we are not able to further improve our computation in this regard. Generally speaking, the agreement of our prediction with Morrell's data is reasonably good.

4.2. Axial interface heat flux distributions

The axial distributions of convective, radiant, sensible and latent heat flux (denoted by q_c, q_r, q_s and q_l respectively) at the gas–liquid interface in the liquid film cooling region with thermally insulated boundary condition is illustrated in Fig. 2. The graphic results of Fig. 2 show that in the liquid film cooling region the convective heat flux decreases axially, because of the growth of the boundary layers of temperature and concentration. The radiant heat flux also gradually decreases in the flow direction. This is a direct consequence of the gradual decrease of the averaged gases temperature. The sensible heat flux decreases rapidly in the region near the coolant injection location and is asymptotically close to zero along the chamber. This is due to the increasing of the liquid film temperature and its approaching the interfacial saturated temperature. It is of interest to notice that the latent heat flux increases axially and reaches the maximum at the location about $x/D = 0.5$ and then decreases very slowly after this point. This can be understood by noting the total energy balance equation at the interface, i.e. $q_c + q_r = q_s + q_l$. It is shown in Fig. 2
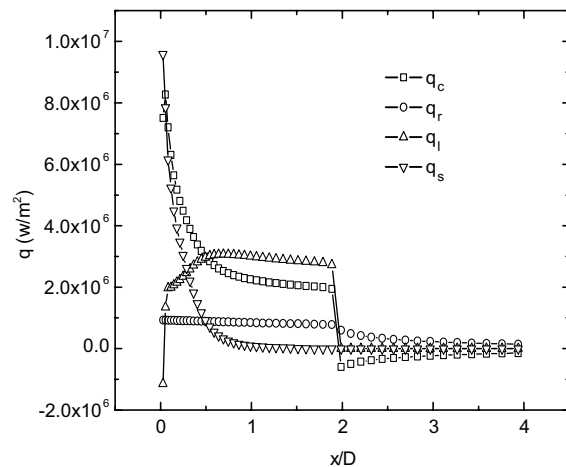
Fig. 2. Distributions of local convective, radiant, sensible, latent heat flux along the chamber ($h = 0$).

that before about $x/D = 0.5$, q_s decreases more rapidly than q_c, while the q_r decreases very slowly, so q_l increases gradually in this region. After about $x/D = 0.5$, however, with the developing of the temperature boundary layer and the closing of the liquid film temperature to the saturation temperature, q_l decreases very slowly and almost levels off. Averagely speaking, under the complicated conditions considered, the radiant heat flux account for about 30% of convective heat flux, and sensible heat flux account for about 35% of the latent heat flux.

To reveal the feature of heat transfer in the whole chamber, the distributions of convective, radiant, sensible and latent heat flux at the chamber wall after the liquid film dry-out point (about $x/D = 2$) are also illustrated in Fig. 2. It is obvious that both the sensible and latent heat flux are equal zero. It is interesting to notice that in this region convective heat flux becomes negative and reaches a new balance with radiant flux. The negative values of convective heat flux indicate that the direction of the convection heat transfer is from the chamber wall to the gas near the wall. This is attributed to the fact that the radiation of the central high temperature gases leads to the increase of the wall temperature,

whereas the temperature of the mixed gases near the wall is relatively low because of the evaporation of the liquid film in the proceeded region. Hence the wall temperature become higher than the gases temperature near the wall, which causes the convective heat transfer from chamber wall to the mixed gases near the wall. It should be noted that it is the low temperature of the vapor–gas mixture adjacent to the wall that cool the chamber wall effectively, from which the terminology of "gaseous film cooling" comes.

To study the effect of regeneration cooling on heat transfer in the combustion chamber, the Rubin thermal boundary condition, i.e., the third kind of boundary condition, is also considered at the outside of the chamber wall. Fig. 3 shows the axial distributions of convective, radiant, sensible and latent heat flux at the gas–liquid interface. All the computational conditions are the same as that for Fig. 2 except for the thermal boundary condition at the wall of the chamber. The heat transfer coefficient of the external cooling was prescribed as $h = 1 \times 10^4 \, \text{W}/(\text{m}^2 \, \text{K})$ in the computation. By comparing Fig. 3 with Fig. 2 it can be found that the sensible heat flux increases evidently. For this case the sensible heat flux includes two parts, one part is absorbed by the liquid film, and other part, which takes up great percentage of sensible heat flux, transfers to outer coolant through the wall. The latent heat flux decreases accordingly, because some energy formerly evaporating liquid film is now lost through the wall. It is interesting to notice that the convection heat transfer increases too. This demonstrates that enhanced evaporation will restrain the convection heat transfer and vice versa. In summary, the total effect of strengthening external cooling on the liquid film is to reduce its evaporation speed and result-ing in increase of the liquid film length. This will be discussed in detail in following section.
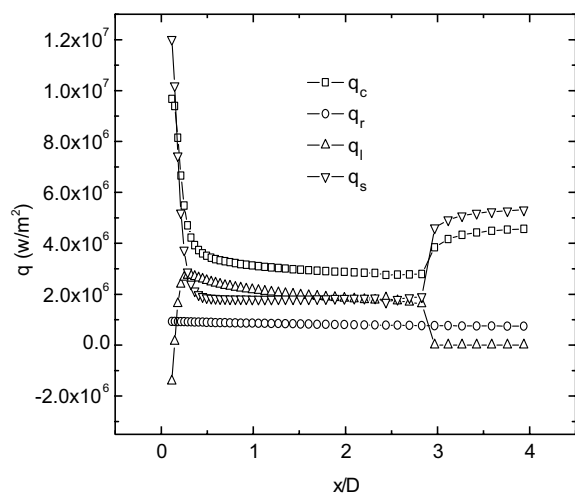
4.3. Distributions of temperature at the wall and interface

Fig. 4 shows the distribution of temperature at the interface and wall. It is clearly that there are the same temperature distributions at the interface for different external heat transfer coefficient. At the inlet region of the chamber the interfacial temperature increases quickly at first and soon arrives the saturated temperature of the liquid film. The wall temperature distribution patterns are similar for different external heat transfer coefficients with a shorter region of high wall temperature and lower maximum wall temperature for higher heat transfer coefficient. As expected, the wall temperature is always low in the liquid film cooling region and increases sharply just beyond the point of the dry-out of liquid film. Though the external cooling strength has little effect on the wall temperature in the region where the liquid film exists, it affects the liquid film length and the maximum wall temperature in the gas film cooling region.

Fig. 5 shows the wall temperature distribution for different MB, which is the mass flux ratio of liquid film to the free stream gas in the entrance location. In this simulation the mass flux of the free stream gas is constant, the different MB means different mass flux of liquid coolant. It illustrates that different mass flux of liquid film just affects the liquid film length, but has little effect on the wall temperature distribution both at the liquid film cooling region and the subsequent gas film cooling region.

Fig. 3. Distributions of local convective, radiant, sensible, latent heat flux along the chamber ($h = 1 \times 10^4 \, \text{W}/\text{m}^2 \, \text{K}$).
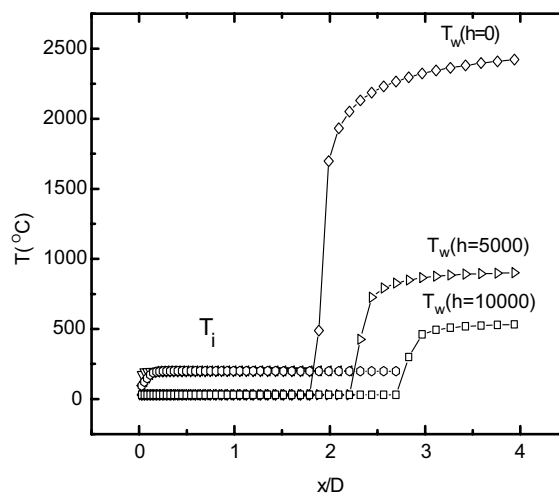
Fig. 4. Distributions of interfacial temperature and wall temperature for different external cooling strength.
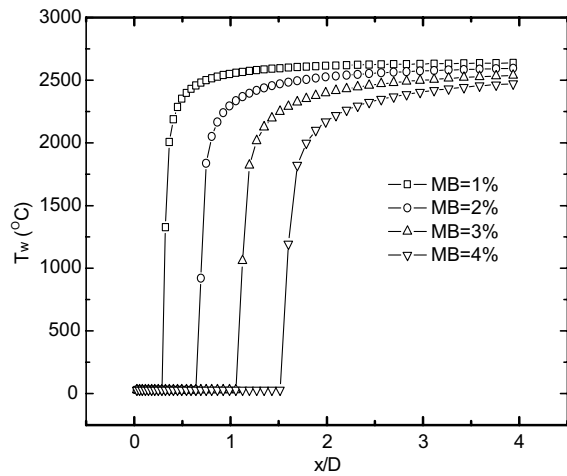
Fig. 5. Distributions of wall temperature for different liquid film mass flux.

4.4. Effect of gas Reynolds number on the liquid film length

To study the effect of the free stream Reynolds number on the liquid film length, two different conditions are considered and the results are shown in Fig. 6. For the condition that Γ is equal to constant, it can be clearly observed that the liquid film length decreases with the increase of the Reynolds number. This attributes to the fact that increasing the Reynolds number means increasing the axial velocity and enhancing the convection heat transfer, and hence, accelerates the liquid film evaporation. Accordingly, the liquid film length decreases with a given mass flux of the liquid film. For
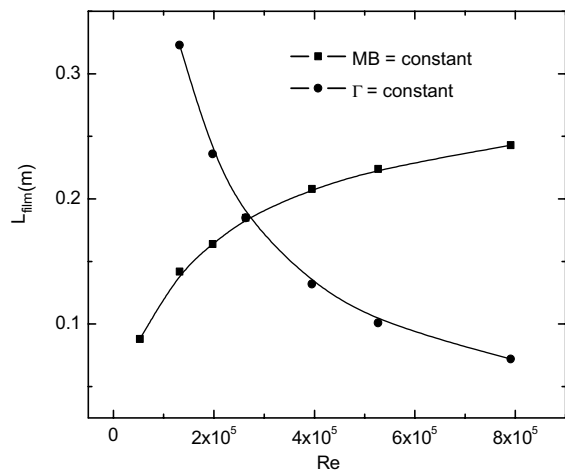
the condition with an invariable MB, Fig. 6 shows that the liquid film length increases with the increase of the Reynolds number. Increase of the liquid film mass flux with constant MB directly leads to the increase in the gas Reynolds number, while increase of the free stream Reynolds number mainly strengthens the convection with an insignificant effect on the gas radiation. Therefore, the effect of the gas radiation is relatively weakened with the Reynolds number increase and vice versa. This is why the liquid film length elongates with the increase of the gas stream Reynolds number under constant MB condition.

4.5. Effect of the external cooling and the coolant inlet temperature on the liquid film length

Fig. 7 shows the effects of the external cooling intensity and the inlet temperature of the liquid coolant on the liquid film length. The results indicate that the liquid film length increases with increase of the external heat transfer coefficient. This is easy to be understood by noting that more heat transfers to external coolant through the wall with strengthening the external cooling. Accordingly, the heat that goes to heating and vaporizing the liquid film becomes less, and the liquid film length increases consequently. Fig. 7 also demonstrates that the liquid film length reduces with the increase in the inlet coolant temperature. This is a consequence of the decrease in the sensible heat: as the inlet coolant temperature increases less heat goes to heating the film and more heat goes to vaporize the liquid film, leading to a shorter liquid film length. However, the effect of the coolant inlet temperature on the liquid film length is less significant

Fig. 6. Effects of Reynolds number on the liquid film length for MB = constant and Γ = constant.
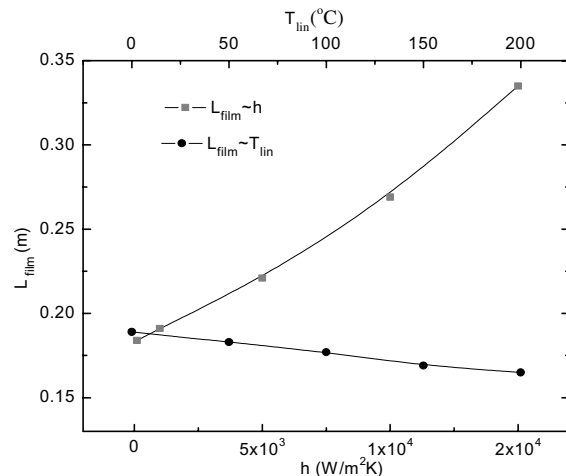
Fig. 7. Effects of inlet coolant temperature and external cooling intensity on the liquid film length.

in comparison with the effect of the external cooling intensity.

5. Conclusions

The liquid film cooling in a rocket combustion chamber has been studied numerically by solving the respective governing equations for the liquid film and the gas stream coupled through the interfacial matching conditions. Based on the numerical results obtained, the following conclusions can be drawn.

(1) Heat transfer at the gas–liquid interface in a rocket combustion chamber with insulated wall is mainly dominated by convection of the free stream and transport of latent heat associated with the evaporation of the liquid film. Meanwhile, the effects of the radiation and sensible heat transfer cannot be ignored. When the wall is cooled by an external coolant, however, the sensible heat transfer become significant, and accordingly the convective heat transfer increases and latent heat flux decreases, leading to the elongation of the liquid film length.

(2) With the increase in the distance from the inlet, the convective, radiant and sensible heat fluxes decrease, but latent heat flux increases at first and then decreases gradually.

(3) The interfacial temperature increases quickly in the entrance region and soon arrives at the saturate temperature of the liquid film. The wall temperature is very low in the liquid film cooling region and increases sharply just beyond the point of the dry-out. Different mass flux of liquid film and external cooling strength have little effect on the wall temperature in the liquid film cooling region. However, both of them affect the liquid film length which determines the length of the gas film cooling region where the wall temperature is quite high.

(4) The liquid film length decreases with the increase of the gas stream Reynolds number for the condition with an invariable coolant mass flux, and the reverse is true for the condition with an invariable mass flux ratio of coolant to the free stream gases at the inlet.

(5) The liquid film length increases with the increase of the external cooling intensity but decreases with increasing the coolant inlet temperature.

References

[1] T. Ueda, H. Tanaka, Measurements of velocity, temperature and fluctuation distributions in liquid films, Int. J. Multiphase Flow 2 (1975) 261–272.

[2] F.K. Wasden, A.E. Dukler, Insights into the hydrodynamics of free falling wavy films, AIChE J. 135 (1989) 187–195.

[3] G.R. Kinney, A.E. Abramson, J.L. Sloop, Internal liquid film cooling experiments with air stream temperatures to 2000 F in 2- and 4-inch diameter horizontal tubes, NACA Report, 1952.

[4] E.L. Knuth, The mechanics of film cooling, JPL Memo, September 1953, pp. 20–85.

[5] M.G. William, Liquid film cooling in rocket engines, CD Report, March 1991.

[6] W.M. Yan, T.F. Lin, Y.L. Tsay, Evaporative cooling of liquid film through interfacial heat and mass transfer in a vertical channel: I—Experimental study, Int. J. Heat and Mass Transfer 34 (1991) 1105–1111.

[7] J. Schroppel, F. Thiele, On the calculation of momentum, heat and mass transfer in laminar and turbulence boundary layer along a vaporizing liquid film, Numer. Heat Transfer 6 (1983) 475–496.

[8] L.C. Chow, J.N. Chung, Evaporation of water into a laminar stream of air and superheated steam, Int. J. Heat Mass Transfer 26 (1983) 373–380.

[9] A.G. Fedorov, R. Viskanta, A.A. Mohamad, Turbulent heat and mass transfer in asymmetrically heated, vertical parallel-plate channel, Int. J. Heat Fluid Flow 18 (1997) 307–315.

[10] T.F. Lin, C.J. Chang, W.M. Yan, Analysis of combined buoyancy effects of thermal and mass diffusion on laminar forced convection heat transfer in a vertical tube, ASME J. Heat Transfer 110 (1991) 337–344.

[11] T.R. Shembharkar, B.R. Pai, Prediction of film cooling with a liquid coolant, Int. J. Heat and Mass Transfer 29 (1986) 899–908.

[12] W.W. Baumann, F. Thiele, Heat and mass transfer in evaporating two-component liquid film flow, Int. J. Heat Mass Transfer 33 (1990) 267–273.

[13] S. He, P. An, J. Li, J.D. Jackson, Combined heat and mass transfer in uniformly heated vertical tube with water film cooling, Int. J. Heat Fluid Flow 19 (1998) 401–417.

[14] W. Nusselt, Die Oberflachenkondensation des Wasserdamphes, Z. VDI 60 (1916) 541–546, 569–575.

[15] W.M. Yan, T.F. Lin, Combined heat and mass transfer in natural convection between vertical parallel plates with film evaporation, Int. J. Heat Mass Transfer 33 (1990) 529–541.

[16] Y.L. Tsay, T.F. Lin, W.M. Yan, Cooling of falling liquid film through interfacial heat and mass transfer, Int. J. Multiphase Flow 16 (1990) 853–865.

[17] W.M. Yan, T.F. Lin, Evaporative cooling of liquid film through interfacial heat and mass transfer in a vertical channel: II—Numerical study, Int. J. Heat Mass Transfer 34 (1991) 1113–1124.

[18] W.M. Yan, C.Y. Soong, Numerical study of liquid film cooling along an inclined plate, Warme-und Stoffubertragung 28 (1993) 233–241.

[19] M'barek Feddaoui, El Mustapha Belahmidi, Ahmed Mir, Abdelaziz Bendou, Numerical study of the evaporative

cooling of liquid film in laminar mixed convection tube flows, Int. J. Therm. Sci. 40 (2001) 1011–1020.

[20] S.M. Yih, J.L. Liu, Prediction of heat transfer in turbulent falling liquid films with or without interfacial shear, AIChE J. 29 (1983) 903–909.

[21] W.M. Yan, Binary diffusion and heat transfer in mixed convection pipe flows with film evaporation, Int. J. Heat Mass Transfer 36 (1993) 2115–2123.

[22] W.M. Yan, C.Y. Soong, Numerical study of liquid film cooling in a turbulent gas stream, Int. J. Heat Mass Transfer 36 (1993) 3877–3885.

[23] W.M. Yan, C.Y. Soong, Convective heat and mass transfer along an inclined heated plate with film evaporation, Int. J. Heat Mass Transfer 38 (1995) 1261–1269.

[24] W.M. Yan, Evaporative cooling of liquid film in turbulent mixed convection channel flows, Int. J. Heat Mass Transfer 41 (1998) 3719–3729.

[25] E.E. Khalil, Modelling of Furnaces and Combustors, Abacus Press, Kent, 1982, pp. 207–208.

[26] W.Q. Tao, Numerical Heat Transfer, second ed., Xi'an Jiaotong University Press, Xi'an, 2001, pp. 96–98.

[27] G. Morrell, Investigation of internal film cooling of 1000 lb thrust liquid ammonia, liquid oxygen rocket engine combustion chamber, NACA RME51E04, July 1951.

[28] N.B. Vargaftik, Tables on the Thermophysical Properties of Liquid and Gases in Normal and Dissociated States, Hemisphere Publishing Corporation, 1975.

[29] R.C. Reid, T.K. Sherwook, The Properties of Gases and Liquids, McGraw-Hill, New York, 1966.

[30] B.E. Launder, D.B. Spalding, The numerical computation of turbulence flows, Comput. Methods Appl. Mech. Eng. 3 (1974) 269–289.

[31] C.C. Chieng, B.E. Launder, On the calculation of turbulent heat transport downstream from an abrupt pipe expansion, Numer. Heat Transfer 3 (1980) 189–207.